

On multiple scatterings of mesons in hot and cold QCD matter

Fabio Dominguez,^{1,*} Cyrille Marquet,^{2,1,†} and Bin Wu^{3,1,‡}

¹*Department of Physics, Columbia University, New York, NY 10027, USA*

²*Service de Physique Théorique, CEA/Saclay, 91191 Gif-sur-Yvette cedex, France*

³*Department of Physics, Peking University, Beijing, 100871, P.R. China*

We study the propagation of a color singlet $q\bar{q}$ pair undergoing multiple scatterings in hot and cold QCD matter. The interaction of the dipole with the nucleus or plasma is described with the McLerran-Venugopalan and Gyulassy-Wang models respectively. We find identical results when expressed in terms of the saturation momentum of either the nucleus or the plasma. We compare two kinds of multiple scatterings, elastic and inelastic with respect to the target. When allowing the target to scatter inelastically, the difference with the elastic case is suppressed by a $1/N_c^2$ factor. We also discuss some implications of our results in the following situations: the survival probability of quarkonia in a hot medium, the production of high- p_T heavy mesons in nucleus-nucleus collisions, and the production of vector mesons in deep inelastic scattering off nuclei.

PACS numbers: 11.80.La, 12.38.Mh, 21.65.Jk

*Electronic address: fabio@phys.columbia.edu

†Electronic address: cyrille@phys.columbia.edu

‡Electronic address: bw2246@columbia.edu

I. INTRODUCTION

The problem of meson dissociation in QCD matter is of great importance in relativistic heavy-ion collisions. Indeed one of the goals of such collisions is to create and understand the quark gluon plasma (QGP) [1], and for many of the possible QGP signatures, the dissociation of mesons in hot or cold matter is involved at some stage. Understanding the mechanisms of meson dissociation is crucial in order to establish a quantitative description of the QGP. It is therefore important to establish how a fast moving bound state is broken apart due to the presence of QCD matter.

One of the important experimental signature of the QGP formation in heavy ion collisions is the suppressed production of high- p_{\perp} hadrons. In standard medium-induced energy loss calculations [2], it is assumed that the partons from the hard scattering hadronize outside of the medium, and therefore that only the energy loss of partons is responsible for jet quenching. However for heavy D and B mesons, whose formation time is less than that of pions, hadronization can happen in the medium, and the problem of meson dissociation in QCD matter becomes relevant. Perhaps this could help improve the description of heavy-meson suppression [3], which is underestimated in the standard picture [4], even after the inclusion of collisional energy loss [5].

Another measurement which is not yet fully understood is the suppressed production of quarkonia [6]. Strong J/Ψ suppression has been observed in nucleus-nucleus collisions by a number of experiments, and various theoretical explanations have been proposed. The natural explanation invoked is the Debye screening [7]: a bound state dissociates because the attractive force between its quark and antiquark is weakened by the color screening caused by the QGP constituents, thermalized quarks and gluons.

However, J/Ψ suppression is also seen in hadron-nucleus collisions and it turns out that cold nuclear matter effects are crucial [8] (note that the mechanisms of heavy quarkonium production in the vacuum are already quite involved [9]). The suppression seen in nucleus-nucleus collision is likely due to the interplay between Debye screening, cold nuclear matter effects [10, 11], and other phenomena such as recombination [12] or another mechanism for meson dissociation: multiple scatterings in the QGP. Interestingly enough, it has recently been shown that for infinite-extend matter, multiple scatterings (collisional dissociation) are a more efficient way of dissociating bound states than Debye screening [13].

Concerning cold nuclear matter effects, it is important to understand them in order to distinguish to what extent experimental observations in heavy-ion collisions are due to initial-state or final-state effects. In the case of quarkonium production, cold matter effects have their own interest, they are relevant for vector meson production in deep inelastic scattering off nuclei at high energies, where large gluon densities in the nucleus are probed [14]. This is an important part of the physics program at a future electron-ion collider [15].

In this work we focus on the multiple scatterings. This is the natural mechanism for meson dissociation in cold nuclear matter, and the dominant one in hot matter for a long enough medium. Having in mind high-energy mesons, we will work within the eikonal approximation. This is suited to discuss forward meson production in hadronic collisions involving only cold matter, and high- p_T production in heavy-ion collisions creating hot matter. We describe the interaction of the mesons with the target nucleus or plasma with the McLerran-Venugopalan (MV) [16] and Gyulassy-Wang (GW) [17] models respectively. We find that multiple scatterings of mesons are very similar in cold and hot matter, they are controlled by the saturation momentum, of either the nucleus or the plasma. This scale determines whether the meson sees a dense or dilute gluon density. We investigate in details the differences between elastic and inelastic scatterings of the target.

The case where the target scatters elastically has been well studied, it only involves the calculation of a two-point function. The situation where one allows the target to break up has not received much attention, and this mechanism is the focus of this paper. It involves the derivation of a four-point function, which is the main technical result of this paper. While several four-point functions have been obtained in the literature [18, 19, 20], the one computed in this paper is new. A general algebraic derivation is explained, and in the large N_c -limit a diagrammatic derivation is also given.

The plan of the paper is as follows. In Section II, we show how the survival probability of a meson in a plasma and the production of vector mesons in deep inelastic scattering are related to a two-dipole correlator, in the eikonal approximation. In Section III, we compute this correlator in the MV model for cold nuclear matter and in Section IV this is done in the GW model for hot QCD matter with an emphasis on the large N_c limit. Section V is devoted to discussions on possible consequences for the dissociation of quarkonia in the QGP, the suppressed production of heavy-mesons in nucleus-nucleus collisions, and for the production of vector mesons in electron-ion collisions. Section VI concludes.

II. DIPOLE SCATTERING IN THE EIKONAL APPROXIMATION

In this section we derive the scattering matrix element between two $q\bar{q}$ color singlet dipole states. This is relevant for the calculation of the survival probability of a meson in a plasma, or the production of vector mesons in deep inelastic scattering. In both cases, these processes involve the two wave functions describing the fluctuation of the initial and final states into $q\bar{q}$ dipoles, and the \hat{S} matrix element between the dipole states. We review the formalism in the eikonal approximation.

We shall use light-cone coordinates with the incoming particle being a right mover. Using light-cone perturbation theory (for an introduction see [21]) and neglecting higher Fock components, we write the $q\bar{q}$ dipole wave function of a meson or virtual photon with tri-momentum $P = (P^+, P_\perp)$ and polarization λ :

$$|P, \lambda\rangle = \int \frac{d^3p}{(2\pi)^3} \phi_{h\bar{h}}^\lambda(p_\perp, z) \frac{\delta_{c\bar{c}}}{\sqrt{N_c}} |p_\perp, z, h, c; P_\perp - p_\perp, 1 - z, \bar{h}, \bar{c}\rangle, \quad (1)$$

where $p = (zP^+, p_\perp)$ denotes the momentum of the quark, z is the fraction of longitudinal momentum P^+ carried by the quark, c and \bar{c} are color indices, and h and \bar{h} are polarization indices.

The normalization of the $q\bar{q}$ state is

$$\langle P', \lambda' | P, \lambda \rangle = (2\pi)^3 2P^+ \delta^{(3)}(P' - P) \delta^{\lambda\lambda'} \sum_{h\bar{h}} \int \frac{d^2p_\perp dz}{16\pi^3} |\phi_{h\bar{h}}^\lambda(p_\perp, z)|^2, \quad (2)$$

where the photon wave function is calculated in QED and is not normalized to unity, while the wave function for the meson is calculated in various models and required to be normalized to unity, meaning:

$$\sum_{h\bar{h}} \int \frac{d^2p_\perp dz}{16\pi^3} |\phi_{h\bar{h}}^\lambda(p_\perp, z)|^2 = 1. \quad (3)$$

The \hat{S} -matrix element $\langle P' | \hat{S} | P \rangle$ is

$$S_{fi} = \frac{1}{N_c} \int \frac{d^3p}{(2\pi)^3} \frac{d^3p'}{(2\pi)^3} \phi_f^*(p'_\perp, z') \phi_i(p_\perp, z) S_{dc}^q(p \rightarrow p') S_{cd}^{\bar{q}}(P - p \rightarrow P' - p'), \quad (4)$$

where S^q and $S^{\bar{q}}$ correspond to the scattering of the quark and antiquark respectively, and d and c are color indices. In formula (4), the polarization indices of the wave function are kept implicit, spins are conserved during the eikonal interaction and are not relevant. In fact the only quantum number changing is the color. The transverse momenta of the partons also

changes however in the high-energy limit, when the partons propagate through the hot or cold matter, they have frozen transverse coordinates and the matrix element depends only of those transverse coordinates. Therefore it is convenient to introduce the wave function and scattering matrix element in a mixed representation (x_\perp, z) with $x_\perp \equiv x_{q\perp} - x_{\bar{q}\perp}$:

$$\phi(p_\perp, z) = \int d^2x_\perp \exp \left\{ -ix_\perp \cdot \left(p_\perp - \frac{m_q}{m_q + m_{\bar{q}}} P_\perp \right) \right\} \varphi(z, x_\perp) , \quad (5)$$

$$S_{dc}^q(p \rightarrow p') = 2\pi \delta(zP^+ - z'P^+) \int d^2x_{q\perp} e^{i(p_\perp - p'_\perp) \cdot x_{q\perp}} W_{dc}(x_{q\perp}) , \quad (6)$$

where $\left(p_\perp - \frac{m_q}{m_q + m_{\bar{q}}} P_\perp \right)$ is the transverse momentum conjugate to x_\perp . The Fourier transformation (5) is defined such that the P^+ dependence in φ only enters through $z = p^+/P^+$, and such that there is no residual P_\perp dependence in $\varphi(z, x_\perp)$. In formula (6), the scattering of the quark is described by the fundamental Wilson line (see for instance [22])

$$W[\mathcal{A}](x_\perp) = \mathcal{P} \exp \left(ig_S \int dz^+ T^c \mathcal{A}_c^-(z^+, x_\perp) \right) \quad (7)$$

where \mathcal{P} denotes an ordering in z^+ . This matrix in color space is a function of the classical color field \mathcal{A}^- (we work in the gauge $\mathcal{A}^+ = 0$) describing the QCD matter. The properties of this color field will be discussed in more detail in the following section. The scattering of the antiquark is described by the Wilson line $W_{cd}^\dagger(x_{\bar{q}\perp})$.

This allows us to write

$$S_{fi} = 2\pi 2P^+ \delta(P'^+ - P^+) M \quad (8)$$

$$M = \int \frac{dz}{4\pi} d^2x_\perp d^2X_\perp e^{i(P_\perp - P'_\perp) \cdot X_\perp} \varphi_f^*(z, x_\perp) \varphi_i(z, x_\perp) S_{q\bar{q}}(x_{q\perp}, x_{\bar{q}\perp}) . \quad (9)$$

The coordinate variables x_\perp and X_\perp are the dipole size and center of mass respectively, they are defined in terms of the quark and antiquark coordinates $x_{q\perp}$ and $x_{\bar{q}\perp}$ in the following way:

$$x_\perp = x_{q\perp} - x_{\bar{q}\perp} , \quad X_\perp = \frac{m_q x_{q\perp} + m_{\bar{q}} x_{\bar{q}\perp}}{m_q + m_{\bar{q}}} . \quad (10)$$

The dipole scattering matrix $S_{q\bar{q}}$ is a trace of Wilson lines:

$$S_{q\bar{q}}(x_{q\perp}, x_{\bar{q}\perp}) = \frac{1}{N_c} \text{Tr} [W(x_{q\perp}) W^\dagger(x_{\bar{q}\perp})] . \quad (11)$$

Introducing the transverse and longitudinal overlap functions between the $q\bar{q}$ color singlet states (for completeness we have reintroduced the spin indices)

$$\Phi_{fi}^T(x_\perp) = \frac{1}{2} \sum_{\lambda=\pm 1} \int \frac{dz}{4\pi} \sum_{h\bar{h}} \varphi_{h\bar{h},f}^{\lambda*}(z, x_\perp) \varphi_{h\bar{h},i}^\lambda(z, x_\perp) , \quad (12)$$

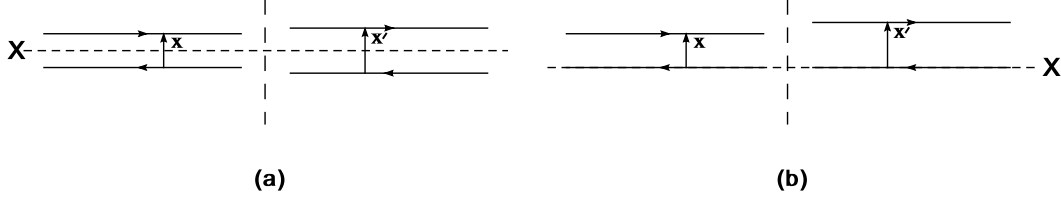


FIG. 1: Two relevant cases which fix the center of mass of the dipoles X_\perp : quarkonia (a) and heavy mesons (b). The dipoles have the same center of mass in the amplitude and the conjugate amplitude because we are integrating over the meson transverse momentum in the final state (14).

and

$$\Phi_{fi}^L(x_\perp) = \int \frac{dz}{4\pi} \sum_{h\bar{h}} \varphi_{h\bar{h},f}^{0*}(z, x_\perp) \varphi_{h\bar{h},i}^0(z, x_\perp), \quad (13)$$

the survival probability of the meson is given by

$$P_{T,L} = \frac{1}{A} \int \frac{d^2 P'_\perp}{(2\pi)^2} \langle |M|^2 \rangle = \int d^2 x_\perp d^2 x'_\perp \Phi_{fi}^{T,L}(x_\perp) \Phi_{fi}^{T,L*}(x'_\perp) \langle S_{q\bar{q}}(x_{q\perp}, x_{\bar{q}\perp}) S_{q\bar{q}}(x'_{q\perp}, x'_{\bar{q}\perp}) \rangle, \quad (14)$$

where $A = \int d^2 X_\perp$ is the cross-sectional area and $\langle \dots \rangle$ represents the medium average which we shall discuss in the following sections. $x'_{q\perp}$ and $x'_{\bar{q}\perp}$ are the quark and antiquark transverse coordinates in the conjugate amplitude:

$$x'_{q\perp} = X_\perp + \frac{m_{\bar{q}}}{m_q + m_{\bar{q}}} x'_\perp, \quad x'_{\bar{q}\perp} = X_\perp - \frac{m_q}{m_q + m_{\bar{q}}} x'_\perp. \quad (15)$$

We have assumed that $\langle \text{Tr} [W^F(x_{a\perp}) W^{F\dagger}(x_{b\perp})] \text{Tr} [W^F(x'_{b\perp}) W^{F\dagger}(x'_{a\perp})] \rangle$ is independent of X_\perp which we justify in the following calculations.

The diffractive production of vector mesons in deep inelastic scattering also involves this dipole-dipole correlator, the cross section reads

$$\sigma_{T,L} = \int d^2 x_\perp d^2 x'_\perp \Phi_{V\gamma}^{T,L}(x_\perp) \Phi_{V\gamma}^{T,L*}(x'_\perp) \int d^2 X_\perp \langle [1 - S_{q\bar{q}}(x_{q\perp}, x_{\bar{q}\perp})][1 - S_{q\bar{q}}(x'_{q\perp}, x'_{\bar{q}\perp})] \rangle, \quad (16)$$

with the appropriate overlap functions $\Phi_{V\gamma}^\lambda$ between the photon and vector meson wave functions. Note that if we replace the correlator $\langle S_{q\bar{q}}(x_{q\perp}, x_{\bar{q}\perp}) S_{q\bar{q}}(x'_{q\perp}, x'_{\bar{q}\perp}) \rangle$, by $\langle S_{q\bar{q}}(x_{q\perp}, x_{\bar{q}\perp}) \rangle \langle S_{q\bar{q}}(x'_{q\perp}, x'_{\bar{q}\perp}) \rangle$, then we are only including scattering processes in which the target scatters elastically, this corresponds to exclusive production. However formula (16) includes the possibility of the target dissociating.

The purpose of this paper is to calculate $\langle S_{q\bar{q}}(x_{q\perp}, x_{\bar{q}\perp}) S_{q\bar{q}}(x'_{\bar{q}\perp}, x'_{q\perp}) \rangle$, and to compare the result with the product of two-point functions $\langle S_{q\bar{q}}(x_{q\perp}, x_{\bar{q}\perp}) \rangle \langle S_{q\bar{q}}(x'_{\bar{q}\perp}, x'_{q\perp}) \rangle$. We shall compute the medium average in the MV model for cold matter, and in the GW model for hot matter, the calculation is essentially the same. The derivation of this 4-point function is the main result of this paper. As pictured in Fig. 1, we will be interested in two particular cases:

- (a) the quarkonium or vector meson case $m_q = m_{\bar{q}}$ meaning:

$$X_{\perp} = \frac{1}{2} (x_{q\perp} + x_{\bar{q}\perp}) = \frac{1}{2} (x'_{q\perp} + x'_{\bar{q}\perp}) , \quad (17)$$

- (b) the heavy meson case $m_{\bar{q}} \gg m_q$, this puts two Wilson lines at the same coordinate, which greatly simplifies the calculation:

$$X_{\perp} = x_{\bar{q}\perp} = x'_{\bar{q}\perp} . \quad (18)$$

Note that we shall only consider quantities integrated over P'_{\perp} , the transverse momentum of the meson in the final state. This is why the two center of masses in the amplitude and the conjugate amplitude are the same (see formula (14)). However, the P'_{\perp} dependence could also be obtained from the results derived in the following.

III. MULTIPLE SCATTERING OF A COLOR SINGLET DIPOLE IN THE MCLERRAN-VENUGOPALAN MODEL

In the Color Glass Condensate framework, the low energy partons of a nuclear wave function, those relevant in high-energy processes, are described by classical color fields. The MV model [16] is a model for the distribution of color charges which generate the field. It is a Gaussian distribution whose variance is the transverse color charge density squared along the projectile's path $\mu^2(z^+)$. The only parameter is the saturation momentum Q_s , with Q_s^2 proportional to the integrated color density squared.

A. Introduction to the MV model

The nuclear average of a function of Wilson lines $f[\mathcal{A}]$ reads

$$\langle f[\mathcal{A}] \rangle = \int D\rho \exp \left(- \int d^2x d^2y dz^+ \frac{\rho_c(z^+, x) \rho_c(z^+, y)}{2\mu^2(z^+)} \right) f[\mathcal{A}] , \quad (19)$$

where the color charge ρ_c and the field \mathcal{A}_c^- obey the Yang-Mills equation

$$-\nabla^2 \mathcal{A}_c^-(z^+, x) = g_S \rho_c(z^+, x) . \quad (20)$$

The MV distribution is a Gaussian distribution, therefore one can compute any average by expanding the Wilson lines in powers of $g_S \rho_c$ and using Wick's theorem. All correlators of ρ 's can be written in terms of

$$\langle \rho_c(z^+, x) \rho_d(z'^+, y) \rangle = \delta_{cd} \delta(z^+ - z'^+) \delta^{(2)}(x - y) \mu^2(z^+) . \quad (21)$$

Note that we dropped the \perp indices denoting transverse vectors, in order to get lighter expressions in the following.

Inverting equation (20) gives \mathcal{A}_c^- in terms of ρ_c :

$$\mathcal{A}_c^-(z^+, x) = g_S \int d^2z G(x - z) \rho_c(z^+, z) , \quad G(x) = \int_{|k| > \Lambda_{QCD}} \frac{d^2k}{(2\pi)^2} \frac{e^{ik \cdot x}}{k^2} , \quad (22)$$

where G is the two-dimensional massless propagator. After expanding the Wilson lines and applying Wick's theorem, every contribution is a product of correlators like

$$g_S^2 \langle \mathcal{A}_c^-(x^+, x) \mathcal{A}_d^-(y^+, y) \rangle = \delta_{cd} \delta(x^+ - y^+) \mu^2(x^+) g_S^4 \int d^2z G(x - z) G(y - z) \quad (23)$$

$$\equiv \delta_{cd} \delta(x^+ - y^+) \mu^2(x^+) L_{xy} \quad (24)$$

times a trace of color matrices. The color algebra is the difficult part to deal with.

B. The dipole-dipole correlator

We now compute the following average

$$\langle S_{q\bar{q}}(x, y) S_{q\bar{q}}(u, v) \rangle . \quad (25)$$

Let's represent each W by a line along the z^+ direction, at a given transverse coordinate. Due to their respective z^+ ordering, W 's are oriented to the right and W^\dagger 's to the left. Due to the color structure, the lines are connected as shown in the left diagram of Fig. 2. Let's expand the Wilson lines in and use Wick's theorem. Graphically, every $\langle \mathcal{AA} \rangle$ correlator (given by (24)) can be represented by a gluon link between two Wilson lines, at the relevant time z^+ , and the factor associated with it is $\mu^2(z^+) L_{xy}$ with x and y the transverse positions of the Wilson lines. This comes with a minus sign if the line is between two (anti)quarks.

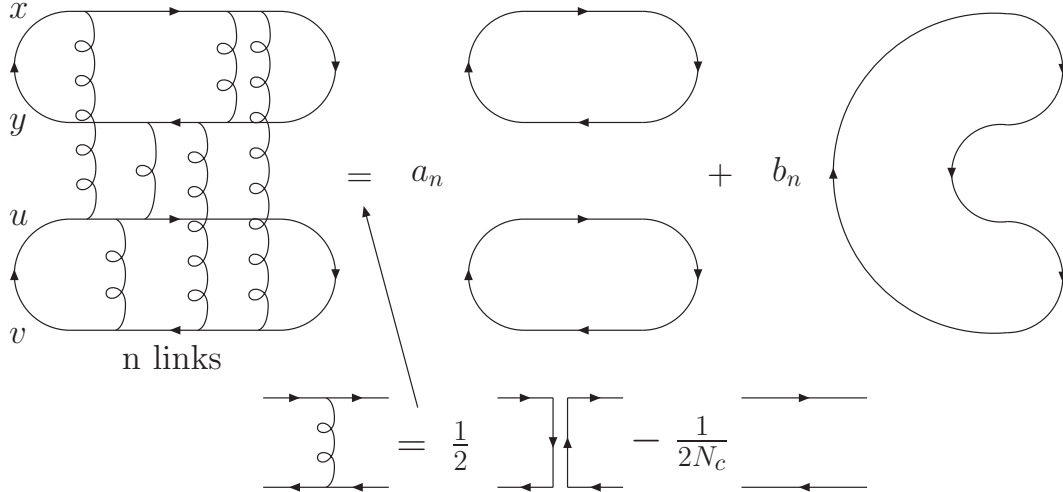


FIG. 2: On the left is a representation of the correlator (25) with an horizontal line for each Wilson line. Each vertical link corresponds to a $\langle \mathcal{A} \mathcal{A} \rangle$ correlator (24) in the $g_S \mathcal{A}$ expansion. The figure shows how, when using the Fierz identify (27), the color structure can be obtained in terms of the two coefficients a_n and b_n . Including diagrams in which a Wilson line is connected to itself, one gets formula (28).

A first class of diagrams, easy to deal with (and shown later in Fig. 6(a)), are those where a Wilson line is connected to itself. Then the contribution is (for instance) $-C_F \mu^2 L_{xx}/2$, it is color singlet and factorizes. The $1/2$ is due to the z^+ ordering in a single Wilson line. Summing contributions with an arbitrary number n of such links (and diving by $n!$ in order not to overcount diagrams) yields

$$T = e^{-\frac{C_F}{2} \mu^2 (L_{xx} + L_{yy} + L_{uu} + L_{vv})} . \quad (26)$$

The second class of diagrams are those where two different Wilson lines are connected, as shown in the figure. Let's simplify their color structure by using

$$T_{ij}^a T_{kl}^a = \frac{1}{2} \delta_{il} \delta_{jk} - \frac{1}{2N_c} \delta_{ij} \delta_{kl} \quad (27)$$

which is represented by the lower diagram in Fig. 2. In doing so, only two topologies can be obtained, the (x, y) and (u, v) color connections can be flipped into (x, v) and (u, y) , or not, and any diagram is the sum of two contributions.

Therefore one can write

$$\langle S_{q\bar{q}}(x, y) S_{q\bar{q}}(u, v) \rangle = \frac{T}{N_c^2} \sum_{n=0}^{\infty} \int_{z_1^+ < \dots < z_n^+} [N_c^2 a_n(z_1^+, \dots, z_n^+) + N_c b_n(z_1^+, \dots, z_n^+)] . \quad (28)$$

The diagrams have been classified by the number n of links they contain. At each order, the sum of diagrams is made of two contributions. The ones where the color structure is not changed (whose sum is denoted a_n) are multiplied by N_c^2 and the ones where the color structure is flipped (whose sum is denoted b_n) are multiplied by N_c . This is illustrated in Fig. 2. The values of a_n and b_n can be obtained by iteration. The derivation is given in the appendices A of [18] and [23]. The sum of diagrams at order n is given by the sum of diagram at order $n - 1$, times the factor for the n -th link. There are six possibilities to add the n -th link on each of the two classes of diagrams. This gives

$$\begin{pmatrix} a_n \\ b_n \end{pmatrix} = \mu^2(z_n^+) M \begin{pmatrix} a_{n-1} \\ b_{n-1} \end{pmatrix} \quad (29)$$

where the 2×2 matrix is given by

$$M = \begin{pmatrix} (L_{xy} + L_{uv})C_F + \frac{1}{2N_c}F(x, y; u, v) & -\frac{1}{2}F(x, v; u, y) \\ -\frac{1}{2}F(x, y; u, v) & (L_{xv} + L_{uy})C_F + \frac{1}{2N_c}F(x, v; u, y) \end{pmatrix} \quad (30)$$

with

$$F(x, y; u, v) = L_{xu} - L_{xv} + L_{yv} - L_{yu} = g_s^4 \int d^2z [G(x-z) - G(y-z)][G(u-z) - G(v-z)] . \quad (31)$$

The problem has been reduced to finding the eigenvalue λ_{\pm} and eigenvectors of M . Indeed one has

$$\begin{pmatrix} a_n \\ b_n \end{pmatrix} = \left(\prod_{i=1}^n \mu^2(z_i^+) \right) M^n \begin{pmatrix} 1 \\ 0 \end{pmatrix} = \left(\prod_{i=1}^n \mu^2(z_i^+) \right) \begin{pmatrix} a_+ \lambda_+^n + a_- \lambda_-^n \\ b_+ \lambda_+^n + b_- \lambda_-^n \end{pmatrix} \quad (32)$$

with a_{\pm} and b_{\pm} obtained from the eigenvectors of M . The results read:

$$\lambda_{\pm} = \left(\frac{N_c}{4} - \frac{1}{2N_c} \right) (L_{xy} + L_{uv}) + \frac{N_c}{4} (L_{xv} + L_{uy}) + \frac{1}{2N_c} F(x, y; u, v) \pm \frac{N_c}{4} \sqrt{\Delta} \quad (33)$$

$$a_{\pm} = \frac{\sqrt{\Delta} \pm F(x, u; y, v)}{2\sqrt{\Delta}}, \quad b_{\pm} = \mp \frac{F(x, y; u, v)}{N_c \sqrt{\Delta}} \quad (34)$$

$$\Delta = F^2(x, u; y, v) + \frac{4}{N_c^2} F(x, y; u, v) F(x, v; u, y) . \quad (35)$$

Finally, resumming the contributions yields

$$\langle S_{q\bar{q}}(x, y) S_{q\bar{q}}(u, v) \rangle = \frac{T}{N_c^2} \left[N_c^2 \left(a_+ e^{\mu^2 \lambda_+} + a_- e^{\mu^2 \lambda_-} \right) + N_c \left(b_+ e^{\mu^2 \lambda_+} + b_- e^{\mu^2 \lambda_-} \right) \right] \quad (36)$$

with

$$\mu^2 = \int dz^+ \mu^2(z^+) . \quad (37)$$

One can write the final result in the following form

$$\begin{aligned} \langle S_{q\bar{q}}(x, y) S_{q\bar{q}}(u, v) \rangle &= \underbrace{e^{-\frac{C_F}{2}[F(x-y)+F(u-v)]}}_{=\langle S_{q\bar{q}}(x,y) \rangle \langle S_{q\bar{q}}(u,v) \rangle} \left[\left(\frac{F(x, u; y, v) + \sqrt{\Delta}}{2\sqrt{\Delta}} - \frac{F(x, y; u, v)}{N_c^2 \sqrt{\Delta}} \right) e^{\frac{N_c}{4} \mu^2 \sqrt{\Delta}} \right. \\ &\quad \left. - \left(\frac{F(x, u; y, v) - \sqrt{\Delta}}{2\sqrt{\Delta}} - \frac{F(x, y; u, v)}{N_c^2 \sqrt{\Delta}} \right) e^{-\frac{N_c}{4} \mu^2 \sqrt{\Delta}} \right] e^{-\frac{N_c}{4} \mu^2 F(x, u; y, v) + \frac{1}{2N_c} \mu^2 F(x, y; u, v)} \quad (38) \end{aligned}$$

It is given in terms of a single function

$$F(x - y) = \mu^2 (L_{xx} + L_{yy} - 2L_{xy}) = g_s^4 \mu^2 \int d^2 z [G(x - z) - G(y - z)]^2 . \quad (39)$$

Indeed also one has

$$-2\mu^2 F(x, y; u, v) = F(x - u) + F(y - v) - F(x - v) - F(y - u) . \quad (40)$$

Note that for $x = y$ or $u = v$, $F(x, y; u, v) = 0$ and one recovers the single dipole average.

In the function $F(r)$, the infrared cutoff Λ_{QCD} only enters through a logarithm as expected. In the $|r|\Lambda_{QCD} \ll 1$ limit, one has

$$\begin{aligned} \frac{C_F}{2} F(r) &= \frac{g_s^4 C_F}{2\pi} \left(\int dz^+ \mu^2(z^+) \right) \int_{\Lambda_{QCD}}^{\infty} dk \frac{1 - J_0(k|r|)}{k^3} \\ &\simeq \frac{r^2}{4} \underbrace{\frac{g_s^4 C_F}{4\pi} \left(\int dz^+ \mu^2(z^+) \right)}_{\equiv Q_s^2(r)} \log \left(\frac{1}{r^2 \Lambda_{QCD}^2} \right) . \quad (41) \end{aligned}$$

This is the standard definition of the saturation scale in the MV model. In the following, we will neglect the logarithmic dependence of Q_s , meaning

$$F(r) = \frac{Q_s^2}{2C_F} r^2, \quad \mu^2 F(x, y; u, v) = \frac{Q_s^2}{2C_F} (x - y) \cdot (u - v) . \quad (42)$$

Finally, note that this model is easily generalized to hot matter. It is showed in Ref.[13] that by only keeping terms up to first order in k_{\perp}/k_z , the gluon propagator in light-cone gauge for a color charge propagating along the light cone in hot matter is

$$D_R^{\mu\nu} \simeq -\frac{i}{k_{\rho} k^{\rho} - \mu_D^2} \left[g^{\mu\nu} - \frac{\eta^{\mu} k^{\nu} + \eta^{\nu} k^{\mu}}{\eta_{\mu} k^{\mu}} \right], \quad (43)$$

where $\mu_D^2 = \frac{1}{6}g^2T^2(N_c + \frac{N_f}{2})$ and $\eta^\mu = \frac{1}{\sqrt{2}}(1, 0, 0, -1)$. To generalize the MV model to hot matter, we treat the valence parton distribution as recoilless color sources which are localized along the light cone, and in the eikonal approximation, the only change of this model is to redefine $G(x)$ as

$$G(x) = \int \frac{d^2k}{(2\pi)^2} \frac{e^{ik \cdot x}}{k^2 + \mu_D^2}, \quad (44)$$

and the infrared cutoff Λ_{QCD} is replaced by the Debye mass of the thermal plasma. In the next section, we will see our generalized MV model is equivalent to the GW model in light-cone coordinates in light-cone gauge.

C. The quarkonium case

Let us consider the situation where the two dipoles have identical center of mass:

$$x = X + \frac{r}{2} \quad y = X - \frac{r}{2} \quad u = X - \frac{r'}{2} \quad v = X + \frac{r'}{2}. \quad (45)$$

Then one finds

$$F(x, y; u, v) = -\frac{Q_s^2}{2C_F} r \cdot r' \quad F(x, u; y, v) = -\frac{Q_s^2}{8C_F} (r + r')^2 \quad (46)$$

which yields

$$\begin{aligned} \langle S_{q\bar{q}}(r) S_{q\bar{q}}(r') \rangle &= e^{-\frac{Q_s^2}{4}(r^2+r'^2)} \left[\left(\frac{-(r+r')^2/4 + \sqrt{\Delta'}}{2\sqrt{\Delta'}} + \frac{r \cdot r'}{N_c^2 \sqrt{\Delta'}} \right) e^{\frac{Q_s^2}{4} \frac{\sqrt{\Delta'}}{1-1/N_c^2}} \right. \\ &\quad \left. + \left(\frac{(r+r')^2/4 + \sqrt{\Delta'}}{2\sqrt{\Delta'}} - \frac{r \cdot r'}{N_c^2 \sqrt{\Delta'}} \right) e^{-\frac{Q_s^2}{4} \frac{\sqrt{\Delta'}}{1-1/N_c^2}} \right] e^{\frac{Q_s^2}{16} \frac{(r+r')^2}{1-1/N_c^2} - \frac{Q_s^2}{2} \frac{r \cdot r'}{N_c^2 - 1}} \end{aligned} \quad (47)$$

with

$$\Delta' = \frac{(r+r')^4}{16} - \frac{r \cdot r'}{N_c^2} (r-r')^2. \quad (48)$$

The large- N_c limit gives:

$$\begin{aligned} \langle S_{q\bar{q}}(r) S_{q\bar{q}}(r') \rangle &= e^{-\frac{Q_s^2}{4}(r^2+r'^2)} \left[1 - \frac{16}{N_c^2} \frac{(r \cdot r')^2}{(r+r')^4} \left(1 + \frac{Q_s^2 (r+r')^2}{8} \right) \right] \\ &\quad + \frac{16}{N_c^2} \frac{(r \cdot r')^2}{(r+r')^4} e^{-\frac{Q_s^2}{8}(r-r')^2}. \end{aligned} \quad (49)$$

D. The heavy meson case

We now consider the situation where both antiquarks are at the same position:

$$x = X + r \quad y = X \quad u = X \quad v = X + r' . \quad (50)$$

Then one finds

$$F(x, y; u, v) = F(x, u; y, v) = -\frac{Q_s^2}{2C_F} r \cdot r' \quad (51)$$

which significantly simplifies the result:

$$\langle S_{q\bar{q}}(r) S_{q\bar{q}}(r') \rangle = e^{-\frac{Q_s^2}{4}(r^2+r'^2)} \left[\frac{1}{N_c^2} e^{\frac{Q_s^2}{2} r \cdot r'} + \left(1 - \frac{1}{N_c^2} \right) e^{-\frac{Q_s^2}{2} \frac{r \cdot r'}{N_c^2 - 1}} \right] . \quad (52)$$

The large N_c -limit is simply

$$\langle S_{q\bar{q}}(r) S_{q\bar{q}}(r') \rangle = e^{-\frac{Q_s^2}{4}(r^2+r'^2)} \left[1 + \frac{1}{N_c^2} \left(e^{\frac{Q_s^2}{2} r \cdot r'} - 1 - \frac{Q_s^2}{2} r \cdot r' \right) \right] \quad (53)$$

$$= e^{-\frac{Q_s^2}{4}(r^2+r'^2)} - \frac{1}{N_c^2} e^{-\frac{Q_s^2}{4}(r^2+r'^2)} \left(1 + \frac{Q_s^2}{2} r \cdot r' \right) + \frac{1}{N_c^2} e^{-\frac{Q_s^2}{4}(r-r')^2} \quad (54)$$

IV. MULTIPLE SCATTERING OF A COLOR SINGLET DIPOLE IN THE GYULASSY-WANG MODEL

In this section, we use the GW model [17] to deal with the multiple scatterings of a color singlet dipole in hot QCD matter. The special case of heavy-meson dissociation due to multiple scattering is addressed in [3], however the color structure is ignored in that analysis. In the following, we will show that the GW model gives the same results as MV model in terms of the saturation momentum Q_s in the eikonal approximation.

A. Introduction to the GW model

In the GW model, the medium is modeled by an interaction Hamiltonian with $N \rightarrow \infty$ scatterers:

$$H_I(t) = \sum_{i=1}^N \sum_{a_i=1}^{N_c^2-1} \int d^3x \left[\Psi_q^\dagger(x) T^{a_i} V_i(x) \Psi_q(x) + \Psi_{\bar{q}}^\dagger(x) T^{a_i} V_i(x) \Psi_{\bar{q}}(x) \right] \equiv H_q(t) + H_{\bar{q}}(t) . \quad (55)$$

The screened potential

$$V_i(\vec{x}) = \frac{-\alpha}{|\vec{x} - \vec{z}_i|} e^{-\mu_D |\vec{x} - \vec{z}_i|} , \quad (56)$$

or $V_i(\vec{q}) = \frac{-4\pi\alpha}{q^2 + \mu_D^2} e^{-i\vec{q} \cdot \vec{z}_i}$ in momentum space, is characterized by the Debye mass μ_D , and describes the medium in the situation $\mu_D \lambda \gg 1$, with λ the mean free path of a single (anti)quark. Even though we are dealing with multiple scattering of a color singlet $q\bar{q}$ dipole in this paper, we still use the mean free path of a single (anti)quark and treat the quark and antiquark in the dipole wave function as two individual free particles. This approximation is good when the relevant length scale of the medium $L \lesssim \gamma\tau$, the typical time scale in a meson [13]. The assumption $1/\mu_D \ll \lambda$ means that the scatterers are independent of each other and, therefore, completely uncorrelated.

The ensemble average over the transverse positions of the scatterers is defined as

$$\langle \dots \rangle \equiv \sum_{i=1}^N \int \frac{d^2 z_{i\perp}}{A} , \quad (57)$$

and after the medium average, each pair of color indices a_i of the generators T^{a_i} at the position \vec{z}_i in the amplitude and/or the conjugate amplitude is identified as illustrated in Fig. 3(a), which is equivalent to (24) in the MV model. This equivalence enables us to calculate the color structure in the same algebraic way than showed in Sec. III. Instead, in this section we choose to calculate the dipole-dipole correlator in the large- N_c limit, which allows a diagrammatic analysis. We shall calculate the probability $P = \sum_{n=0}^{\infty} P^{(n)}$ in the eikonal approximation with

$$P^{(n)} = \frac{1}{A} \int \frac{d^2 P_{\perp}'}{(2\pi)^2} \langle |M^{(n)}|^2 \rangle , \quad (58)$$

the contribution to P from those diagrams with n scattering centers scattering with the dipole in the amplitude and/or the conjugate amplitude.

Among N scatterers, we have $C_N^n = \frac{N!}{n!(N-n)!} \simeq \frac{N^n}{n!}$ choices of the n scatterers which scatter with the dipole in the amplitude and/or the conjugate amplitude. In the eikonal approximation, each choice of those n scatterers will give the same contribution to $P^{(n)}$. Therefore, let us assume that the dipole, moving along the $+$ direction, is scattered by the first n scatterers which are located at $\vec{z}_i, i = 1, \dots, n$ respectively with $z_i^+ > z_{i-1}^+$. In the following, we enumerate the n scatterers by z_i and by $z_i > z_j$ we mean $z_i^+ > z_j^+$. Focusing on the color factor of each term contributing to $P^{(n)}$, there exists a Feynman diagram with

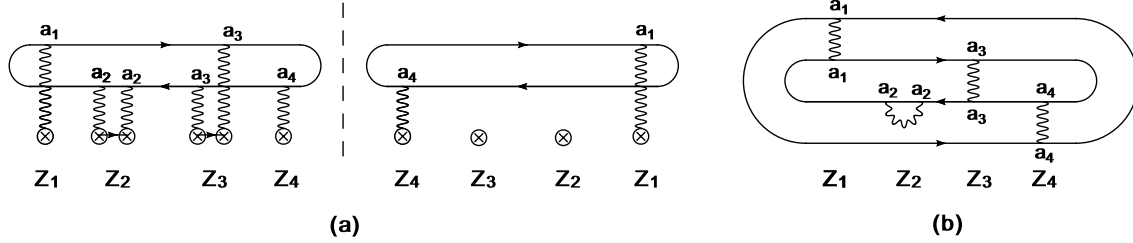


FIG. 3: The equivalence of the color factors between (a) and (b): after the medium average, each pair of color indices a_i of the generators T^{a_i} at the position z_i in the amplitude and/or the conjugate amplitude is identified. Therefore, it has the same color factor as the Feynman diagram (b). In the large N_c limit, the amplitude of (b) is proportional to C_F^2 in contrast with that in Fig. 4(b).

the same color factor. An example is showed in Fig. 3. We will use this correspondence to evaluate P by a diagrammatic analysis at large N_c . Up to $\mathcal{O}(\alpha^2)$, we will evaluate separately the following two cases:

- single-scattering diagrams such as those shown in Fig. 4(a). In this case, since the n scattering centers all scatter with the dipole by single scattering in the amplitude, they must also scatter with it in the conjugate amplitude. This corresponds to processes in which the target scatters inelastically.
- double-scattering diagrams such as those shown in Fig. 3(a). In this case, if the scatterer z_i undergoes double scattering in the amplitude, there must be no scattering between it and the dipole in the conjugate amplitude and vice versa. This corresponds to processes in which the target scatters elastically.

B. The evaluation of single-scattering diagrams

The amplitude for the dipole to undergo n single scatterings with those n scatterers $M_s^{(n)}$ is a sum of 2^n corresponding diagrams since the gluon line from each scatterer can hook either on the quark or the antiquark line. If the gluon line from the scatterer z_i hooks on the quark or the antiquark line, the corresponding amplitude picks up a phase $e^{i\frac{m\bar{q}}{M}q_{\perp i}\cdot x_{\perp}} = e^{iq_{\perp i}\cdot(x_{q\perp} - X_{\perp})}$ or $e^{-i\frac{mq}{M}q_{\perp i}\cdot x_{\perp}} = e^{iq_{\perp i}\cdot(x_{\bar{q}\perp} - X_{\perp})}$ respectively, where $q_{\perp i}$ denotes the transverse momentum of the gluon line. In the mean time, the color matrix T^{z_i} is put in the

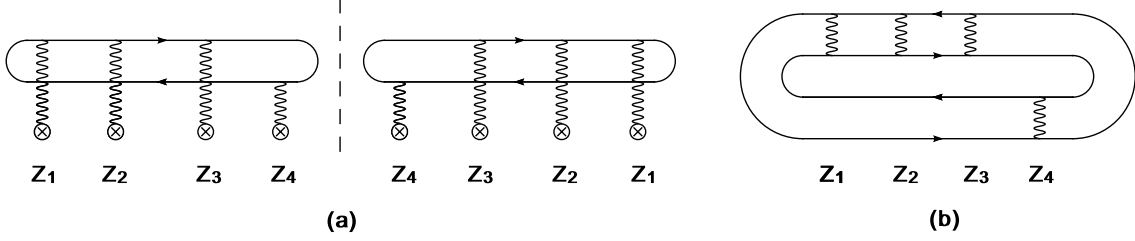


FIG. 4: An example of single-scattering diagram of the leading order in N_c : The contribution of (a) to $P^{(n)}$ has the same color factor as the amplitude of (b), which is proportional to C_F^4 in the large N_c limit.

quark part or antiquark part of the trace of the n color matrices accordingly. For example, if the scatterers $z_{a_1} < \dots < z_{a_m}$ and $z_{b_1} < \dots < z_{b_{n-m}}$ scatter with the quark and antiquark respectively, we have $\text{Tr} [T^{z_{a_m}} \dots T^{z_{a_1}} T^{z_{b_1}} \dots T^{z_{b_{n-m}}}]$ in the amplitude of the corresponding diagram. In general, we have

$$M_s^{(n)} = (i)^n \frac{1}{N_c} \int d^2 x_\perp \Phi_{f_i}^\lambda(x_\perp) \int \prod_{i=1}^{n-1} \left[\frac{d^2 q_{\perp i}}{(2\pi)^2} \right] \times \prod_{i=1}^n \left[\frac{4\pi\alpha e^{-iq_{\perp i} \cdot z_{\perp i}}}{q_{\perp i}^2 + \mu_D^2} \left(e^{i\frac{m_{\bar{q}}}{M} q_{\perp i} \cdot x_\perp} T_{c_{i+1}c_i}^{a_i} \delta_{d_i d_{i+1}} - e^{-i\frac{m_q}{M} q_{\perp i} \cdot x_\perp} T_{d_i d_{i+1}}^{a_i} \delta_{c_i c_{i+1}} \right) \right], \quad (59)$$

with $c_1 = d_1$, $d_{n+1} = c_{n+1}$ and $M = m_q + m_{\bar{q}}$.

In fact, it is easy to show that we only have 2^{n-2} different traces of color matrices in $M_s^{(n)}$ which correspond respectively to the 2^{n-2} different hookings of the gluon lines from the $n-2$ scatterers in between z_1 and z_n on the quark and antiquark lines. Generally, we write the trace in the following form

$$\text{Tr}^{(n,m)} \equiv \text{Tr} [T^{z_n} T^{z_{a_m}} \dots T^{z_{a_1}} T^{z_1} T^{z_{b_1}} \dots T^{z_{b_{n-m-2}}}], \quad (60)$$

and the corresponding four diagrams give to $M_s^{(n)}$ a contribution

$$M_s^{(n,m)} = (i)^n \frac{(-1)^{n-m-2}}{N_c} \text{Tr}^{(n,m)} \int d^2 x_\perp \Phi_{f_i}^\lambda(x_\perp) \int \prod_{i=1}^{n-1} \left[\frac{d^2 q_{\perp i}}{(2\pi)^2} \right] \times \prod_{i=1}^n \left[\frac{4\pi\alpha e^{-iq_{\perp i} \cdot z_{\perp i}}}{q_{\perp i}^2 + \mu_D^2} \right] e^{i\frac{m_{\bar{q}}}{M} \sum_{j=1}^m q_{\perp a_j} \cdot x_\perp - i\frac{m_q}{M} \sum_{j=1}^{n-m-2} q_{\perp b_j} \cdot x_\perp} \times \left(e^{i\frac{m_{\bar{q}}}{M} q_{\perp 1} \cdot x_\perp} - e^{-i\frac{m_q}{M} q_{\perp 1} \cdot x_\perp} \right) \left(e^{i\frac{m_{\bar{q}}}{M} q_{\perp n} \cdot x_\perp} - e^{-i\frac{m_q}{M} q_{\perp n} \cdot x_\perp} \right). \quad (61)$$

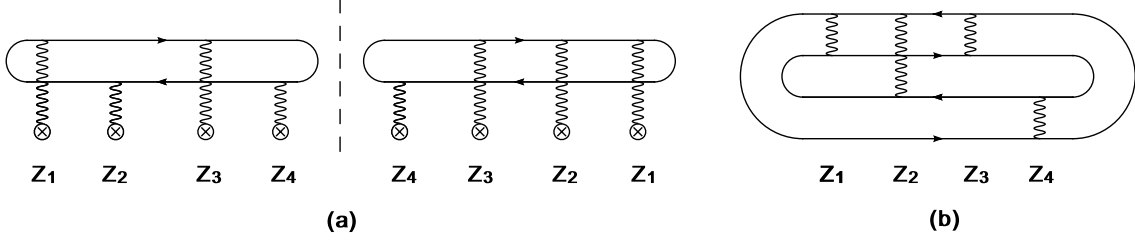


FIG. 5: An example for $1/N_c^2$ suppressed diagram of single-scatterings to $P^{(n)}$: in (a) the gluon line from the scatterer z_2 hooks on different fermion lines in the amplitude and conjugate amplitude. It has the same color factor as the Feynman diagram (b), which is non-planar and $1/N_c^2$ suppressed relative to Fig. 4(b) [24].

In the large N_c limit, to evaluate

$$P_s^{(n)} = C_N^m \frac{1}{A} \int \frac{d^2 P'_\perp}{(2\pi)^2} \langle |M_s^{(n)}|^2 \rangle, \quad (62)$$

we only need to take into account those diagrams with each pair of the $n - 2$ scatterers in between z_1 and z_n hooking on the same fermion line in the amplitude and conjugate amplitude. For example, in the case $n = 4$, the contribution to $P_D^{(n)}$ from the diagram Fig. 4(a) has the same color factor as Fig. 4(b) $\propto C_F^4$, while the color factor of the contribution from Fig. 5(a) correspond to a non-planar diagram Fig. 5(b) and, therefore, are $1/N_c^2$ suppressed relative to Fig. 4(b) [24]. This means that we only need to count in the 2^{n-2} products of $M_D^{(n,m)}$ and their conjugates, which have a unique color factor

$$\text{Tr}[T^{z_n} \dots T^{z_1}] \text{Tr}[T^{z_1} \dots T^{z_n}] = C_F^m + (-1)^n \frac{N_c^2 - 1}{2^n N_c^n} \simeq C_F^m. \quad (63)$$

Therefore, for arbitrary $n \geq 2$, we have in the large N_c limit

$$P_s^{(n)} = \frac{1}{n!} P_2 (Z + 2\chi)^{n-2}, \quad (64)$$

where

$$\begin{aligned} P_2 &\equiv \frac{1}{N_c^2} (L\rho\sigma)^2 \int d^2 x_\perp d^2 x'_\perp \Phi_{fi}^\lambda(x_\perp) \Phi_{fi}^{\lambda*}(x'_\perp) \\ &\times \left[\int d^2 q_\perp \frac{\mu_D^2}{\pi(q_\perp^2 + \mu_D^2)^2} \left(e^{i\frac{m\bar{q}}{M} q_\perp \cdot x_\perp} - e^{-i\frac{m\bar{q}}{M} q_\perp \cdot x_\perp} \right) \left(e^{-i\frac{m\bar{q}}{M} q_\perp \cdot x'_\perp} - e^{i\frac{m\bar{q}}{M} q_\perp \cdot x'_\perp} \right) \right]^2 \\ &\simeq \frac{1}{N_c^2} \int d^2 x_\perp d^2 x'_\perp \Phi_{fi}^\lambda(x_\perp) \Phi_{fi}^{\lambda*}(x'_\perp) \frac{1}{4} Q_s^4(x_\perp \cdot x'_\perp)^2, \end{aligned} \quad (65)$$

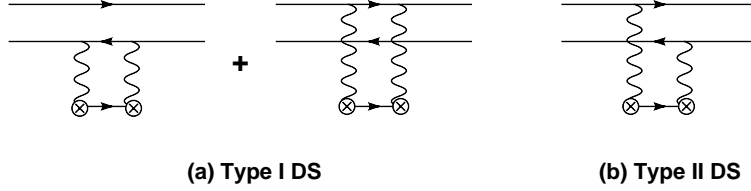


FIG. 6: Two types of double-scatterings for each scatterer in the amplitude: after the medium average the color factor of (a) is trivially C_F while the color factor of (b) depends on its relative position with respect to those for single-scatterings. If it is not in between any two of single-scatterings, it also has a color factor C_F .

and

$$Z \equiv \int d^2 q_{\perp} \frac{L\rho\sigma\mu_D^2}{\pi(q_{\perp}^2 + \mu_D^2)^2} \left(e^{i\frac{m\bar{q}}{M}q_{\perp}\cdot(x_{\perp}-x'_{\perp})} + e^{-i\frac{m q}{M}q_{\perp}\cdot(x_{\perp}-x'_{\perp})} - 2 \right). \quad (66)$$

We have introduced the number density in the transverse plane $\frac{N}{A} = L\rho$ with L the plasma length and ρ the number density of scatterers, the cross section of the (anti)quark undergoing a single scattering $\sigma = \frac{4\pi\alpha^2 C_F}{\mu_D^2}$, and the average scattering number $\chi = \frac{L}{\lambda} = L\rho\sigma$. Finally,

$$Q_s^2 = L\rho\sigma \int_{|q_{\perp}| < 1/|x_{\perp}|} d^2 q_{\perp} \frac{\mu_D^2}{\pi(q_{\perp}^2 + \mu_D^2)^2} q_{\perp}^2 \quad (67)$$

is the plasma saturation momentum squared, which is a characteristic property of the QCD medium. It is different from the traditional saturation momentum introduced in the previous section (which characterizes the small- x part of a hadronic wave function), but when writing (67) in terms of the gluon density per unit of transverse area in the plasma [25], one finds the same expression than when writing the saturation scale in terms of the gluon density per unit of transverse area in a hadron. And indeed, one can check that formula (41) is recovered in the $|x_{\perp}|\mu_D \ll 1$ limit if one replaces μ_D with Λ_{QCD} in (67). In terms of the traditional jet quenching parameter \hat{q} , one has $Q_s^2 = \hat{q}atqL$. Note also that in formula (65), we have assumed that $|q_{\perp} \cdot x_{\perp}| \ll 1$. This is justified because the typical values are $|q_{\perp}| \sim T$ while $|x_{\perp}| \sim a_B$, the meson size. We always assume a situation where $Ta_B \ll 1$, where multiple scatterings are important.

C. The evaluation of double-scattering diagrams

In all the diagrams, we only need to evaluate two types of double-scatterings as showed in Fig. 6. Each type I double-scatterings and its conjugate give a contribution -2χ to $P^{(n)}$. This is easily read out from the corresponding diagrams such as the type I double-scattering at z_2 in Fig. 3(a). Those diagrams with at least one type II double-scattering in between two single-scatterings are $1/N_c^2$ suppressed. For example, the contribution to $P^{(n)}$ corresponding to Fig. 3(a) $\propto C_F^2$ is $1/N_c^2$ suppressed compared with that in Fig. 4(a) in the large N_c limit. Otherwise, each type II double-scattering and its conjugate give to $P^{(n)}$ a contribution

$$Y + 2\chi \equiv \int d^2q_\perp \frac{L\rho\sigma\mu_D^2}{\pi(q_\perp^2 + \mu_D^2)^2} \left(e^{iq_\perp \cdot x_\perp} + e^{-iq_\perp \cdot x_\perp} \right), \quad (68)$$

with

$$Y \simeq -\frac{1}{4}Q_s^2(x_\perp^2 + x_\perp'^2). \quad (69)$$

If the dipole interacts with the medium only through double-scatterings, that is, the target is not excited, we get the probability for the so-called elastic process

$$\begin{aligned} P_{el}^\lambda &= \int d^2x_\perp d^2x'_\perp \Phi_{fi}^\lambda(x_\perp) \Phi_{fi}^{\lambda*}(x'_\perp) \sum_{m_I, m_{II}=0}^{\infty} \frac{1}{m_I! m_{II}!} (-2\chi)^{m_I} (Y + 2\chi)^{m_{II}} \\ &= \int d^2x_\perp d^2x'_\perp \Phi_{fi}^\lambda(x_\perp) \Phi_{fi}^{\lambda*}(x'_\perp) e^{-\frac{1}{4}Q_s^2(x_\perp^2 + x_\perp'^2)}. \end{aligned} \quad (70)$$

D. The survival probability from inelastic multiple scatterings

Now, we are ready to evaluate $P_{inel}^{(n)}$ up to order $1/N_c^2$, the probability for the transition of an initial state φ_i to a final state φ_f undergoing at least $n \geq 2$ single-scatterings with the medium excited. Let us assume that there are m_I type I double-scatterings and m_{II} type II double-scatterings among total n scatterings. First, we have $C_N^n = \frac{N!}{n!(N-n)!} \simeq \frac{N^n}{n!}$ choices of the n scatterers. Then out of those n scatterers, we have $C_n^{n-m_I}$ possible choices of $(n - m_I)$ scatterers undergoing $(n - m_I - m_{II})$ single-scatterings and m_{II} type II double-scatterings. Since we only need to count in the diagrams with no type II double-scattering in between any two of all the $(n - m_I - m_{II})$ single-scatterings, we only have $(m_{II} + 1)$ choices of the m_{II} scatterers undergoing type II double-scattering.

Therefore, for each group (n, m_I, m_{II}) , we have

$$\begin{aligned} P^{(n, m_I, m_{II})} &= \frac{1}{n!} C_n^{n-m_I} (m_{II} + 1) P_2(-2\chi)^{m_I} (Y + 2\chi)^{m_{II}} (Z + 2\chi)^{n-m_I-m_{II}-2} \\ &= \frac{m_{II} + 1}{m_I!(n - m_I)!} P_2(-2\chi)^{m_I} (Y + 2\chi)^{m_{II}} (Z + 2\chi)^{n-m_I-m_{II}-2}, \end{aligned} \quad (71)$$

which leads to

$$P_{inel}^{(n)} = \sum_{m_{II}=0}^{n-2} \sum_{m_I=0}^{n-2-m_{II}} P^{(n, m_I, m_{II})} = \frac{1}{n!} \sum_{m=0}^{n-2} (m+1) Y^m Z^{n-m-2}, \quad (72)$$

and finally

$$P_{inel} = \sum_{n=2}^{\infty} P_{inel}^{(n)} = \frac{P_2}{(Y - Z)^2} [e^Z + (Y - Z - 1)e^Y]. \quad (73)$$

We can now discuss the two situations of Fig. 1 (we recall that $x_{\perp} = x_{q\perp} - x_{\bar{q}\perp}$ and $x'_{\perp} = x'_{q\perp} - x'_{\bar{q}\perp}$).

- (a) In the quarkonium case: $m_{\bar{q}} \simeq m_q$ and $X_{\perp} \simeq (x_{q\perp} + x_{\bar{q}\perp})/2 = (x'_{q\perp} + x'_{\bar{q}\perp})/2$, this leads to $Z = -\frac{Q_s^2}{8}(x_{\perp} - x'_{\perp})^2$ and

$$\begin{aligned} P_{inel}^{\lambda} &= \frac{1}{N_c^2} \int d^2x_{\perp} d^2x'_{\perp} \Phi_{fi}^{\lambda}(x_{\perp}) \Phi_{fi}^{\lambda*}(x'_{\perp}) \\ &\times \left\{ \frac{16(x_{\perp} \cdot x'_{\perp})^2}{(x_{\perp} + x'_{\perp})^4} e^{-\frac{1}{8}Q_s^2(x_{\perp} - x'_{\perp})^2} - \frac{2(x_{\perp} \cdot x'_{\perp})^2}{(x_{\perp} + x'_{\perp})^2} \left[Q_s^2 + \frac{8}{(x_{\perp} + x'_{\perp})^2} \right] e^{-\frac{1}{4}Q_s^2(x_{\perp}^2 + x'_{\perp}^2)} \right\}. \end{aligned} \quad (74)$$

- (b) In the heavy-meson case: $m_{\bar{q}} \gg m_q$, and $X_{\perp} \simeq x_{\bar{q}\perp} = x'_{\bar{q}\perp}$, this leads to $Z = -\frac{Q_s^2}{4}(x_{\perp} - x'_{\perp})^2$ and

$$\begin{aligned} P_{inel}^{\lambda} &= \frac{1}{N_c^2} \int d^2x_{\perp} d^2x'_{\perp} \Phi_{fi}^{\lambda}(x_{\perp}) \Phi_{fi}^{\lambda*}(x'_{\perp}) \\ &\times \left[e^{-\frac{1}{4}Q_s^2(x_{\perp} - x'_{\perp})^2} - \left(1 + \frac{1}{2}Q_s^2 x_{\perp} \cdot x'_{\perp} \right) e^{-\frac{1}{4}Q_s^2(x_{\perp}^2 + x'_{\perp}^2)} \right]. \end{aligned} \quad (75)$$

In both cases, we obtain the same survival probability

$$P_{el}^{\lambda} + P_{inel}^{\lambda} = \int d^2x_{\perp} d^2x'_{\perp} \Phi_{fi}^{\lambda}(x_{\perp}) \Phi_{fi}^{\lambda*}(x'_{\perp}) \langle S_{q\bar{q}}(x_{\perp}) S_{q\bar{q}}(x'_{\perp}) \rangle \quad (76)$$

as in the previous section, the differences enter through the saturation scales only. The infrared scale is Λ_{QCD} in the cold QCD matter case, and μ_D for hot QCD matter.

V. PHENOMENOLOGICAL IMPLICATIONS

It is very interesting to see how the two different approaches, for cold and hot matter, yield the same result when expressed in terms of the appropriate saturation scale. This fact allows us to make general comments about bound state dissociation and vector meson production leaving all the medium dependence in only one parameter. From the calculations shown in previous sections we can easily see that in the large N_c limit, the main contribution to the dipole-dipole correlator comes from elastic processes. The contribution coming from inelastic processes is $1/N_c^2$ suppressed, and is therefore 10 % smaller in general. However, the different dependences of the subleading contributions on the size and orientation of the dipoles can play an important role in determining when these contributions become comparable to the one from the elastic case. For instance, we notice that the elastic correlator (as shown in (70)) is insensitive to the relative orientation of the dipoles but the inelastic contribution is not.

First, it is worth noticing that the inelastic contribution goes to zero as Q_s^4 when Q_s goes to zero both for the heavy meson and the quarkonium case. In this limit which corresponds to turning off the interaction, elastic dissociation goes to zero only as Q_s^2 , therefore in order to get a large contribution from inelastic processes Q_s should be large enough. This observation has to be taken with caution since Q_s is present in all of the exponentials. A too large Q_s induces a big suppression in the dipole-dipole correlator (elastic or inelastic) except for very small dipole sizes, which don't give a big contribution when the wave functions are included (Eq. (14), (16)).

With the above considerations in mind, we can easily notice that the terms in the inelastic part of the correlator with the exponential factor $e^{-\frac{Q_s^2}{4}(x_\perp^2+x'_\perp^2)}$ in Eqs. (74) and (75) don't give a large contribution, since they only become comparable with the elastic part in a region heavily suppressed by the exponential factor and the wave functions. Following this observation we turn our attention to the terms with the exponential factors of the form $e^{-\frac{Q_s^2}{4}(x_\perp-x'_\perp)^2}$ and $e^{-\frac{Q_s^2}{8}(x_\perp-x'_\perp)^2}$. Unlike the other terms, these exponentials are not necessarily small for large dipoles and don't exhibit the property of color transparency, which is characteristic of the elastic terms. As long as the two dipoles are aligned and similar in size, the first term in both expressions for the inelastic part can overcome the $1/N_c^2$ suppression and become comparable with the elastic part.

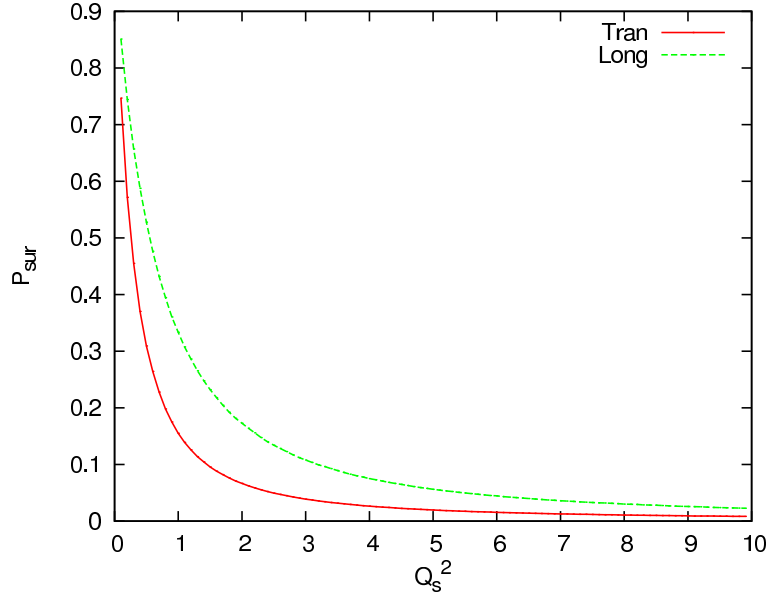


FIG. 7: Survival probabilities for J/ψ mesons, using “light-cone gaussian” wave functions and the dipole-dipole correlator (47).

More precise comparisons of the relative sizes for different dipole configurations require a more intricate numerical analysis which is left for future work, especially the result of the interplay between the size dependences of the meson wave functions and those of the dipole-dipole correlator should be investigated numerically. Still, let us make more specific comments concerning different physical situations where we expect our results to be relevant.

A. Super-penetration of quarkonia

As an example of a full numerical calculation, we considered the J/ψ survival probability. The light-cone wave functions of Ref. [26] were used to obtain the probability plotted in Fig. 7 as a function of Q_s^2 . Current measurements in heavy-ion collisions at RHIC suggest a value of $Q_s^2 \sim 1 \text{ GeV}^2$ for a gold nucleus and $Q_s^2 = \hat{q}L \sim 20 \text{ GeV}^2$ for a plasma with a size of a few fermis for central collisions. At the LHC, these values can be increased by a factor of order 3, given the accessibility to partons with smaller momentum fraction in the nuclear wave function, or higher plasma temperatures in the hot matter case. We can anticipate that the results at the LHC should be qualitatively different since the survival probability decreases by about one order of magnitude.

We also observe on Fig. 7 that the survival probability decreases as $1/Q_s^2$ for large values of Q_s . In the hot matter case, this corresponds to a $1/L$ behavior in terms of the plasma length. This dependence, already derived previously [23] (and in [27, 28] for an $SU(2)$ color group), is in contrast with the e^{-L} decrease usually assumed. Such an exponential dependence is valid when the dipole undergoes successful independent scatterings in the medium, while the power-law we obtain is due to the coherence of the multiple scatterings, and both the elastic and inelastic contributions display this *super-penetration* feature [29]. A similar scaling was also observed when considering the suppressed production of heavy quarks off cold nuclear matter [30].

B. Collisional dissociation of heavy mesons

While for light hadrons, partonic energy-loss calculations can describe the suppressed production of high- p_T particles in nucleus-nucleus collisions at RHIC, the suppression is underestimated in the case of D and B mesons (or rather single non-photonic electrons coming from the decays) [5]. The discrepancy is due to the small quenching of B -mesons, which dominate the high- p_T single electron yields. However, the standard calculations assume that the hard parton hadronizes outside the medium, having fully traversed the region of dense nuclear matter, and lost energy via radiative and collisional processes. But for heavy mesons, due to the significantly smaller formation times, this assumption does not appear to be justified. In fact, it was shown that including collisional dissociation goes in the right direction [3]: contrary to calculations that emphasize radiative and collisional heavy quark energy loss, collisional dissociation predicts that D and B mesons are suppressed in a similar way at transverse momenta as low as $p_T \sim 10$ GeV.

The framework of Ref. [3] takes into account the competition between the fragmentation of c and b quarks and the medium-induced dissociation of the D and B mesons to evaluate the quenching in nucleus-nucleus collisions. The meson survival probability we have computed in the previous sections is an important ingredient of their analysis: it determines the dissociation time of the meson in the plasma. However the expression used in [3] ignores the color structure of the theory and therefore it would be interesting to redo the analysis with our expression, but this is beyond the scope of this work. Note that the time dependence of the plasma formation and evolution is easily implemented by varying the parameter Q_s^2 .

C. Diffractive vector meson production

An experimental situation where elastic and inelastic processes can be distinguished is the diffractive production of vector mesons in deep inelastic scattering: $\gamma^*A \rightarrow VY$, where A stands for the target nucleus and Y for the final state it has dissociated into. In this process, the $q\bar{q}$ pair that the virtual photon has fluctuated into scatters off the nucleus before recombining into a vector meson. While the scattering involves a color-singlet exchange, leaving a rapidity gap in the final state, the nucleus can still scatter elastically ($Y = A$, this is called coherent diffraction) or inelastically (*i.e.* break up, called incoherent diffraction). Kinematically, a low invariant mass of the system Y corresponds to a large rapidity gap between that system and the vector meson (this also implies that the longitudinal momentum of the meson is close to that of the photon, which justifies using the eikonal approximation for this process), which makes it possible in principle to keep track of the state of the target, and separate coherent and incoherent diffraction.

The cross-section is peaked at minimum momentum transfer where the elastic scattering dominates, but as the transfer of momentum gets larger, the role of the inelastic contribution increases and eventually it becomes dominant (typically for momenta bigger than the inverse nucleus size). The momentum transfer in this process is essentially the transverse momentum of the vector meson in the final state P'_\perp , and as a function of $|t| = P'^2_\perp$, the elastic contribution decreases exponentially while the inelastic contribution decreases only as a power law. This important difference was not discussed in this paper where only P'_\perp -integrated quantities are analyzed. It deserves detailed studies which are left for future work, such as for instance the numerical analysis of our results and a comparison with data from HERA on diffractive vector meson production, with or without proton breakup. The case of deep inelastic scattering off a large nucleus should also be studied, and in this case the MV model we considered provides a natural framework, and a good starting point to implement the high-energy QCD evolution. Inclusive and diffractive structure functions have been calculated [31], but vector-meson production has yet to be addressed. At an electron-ion collider, when the momentum transfer is small enough for the nucleus to stay intact, then it will escape too close to the beam to be detectable; therefore the whole diffractive program will rely on our understanding of incoherent diffraction.

VI. CONCLUSIONS

The main technical result of the paper is the 4-point function (38), computed in the MV model for cold nuclear matter, but also valid in the GW model for hot matter. This dipole-dipole correlator allows to compute the survival probability of a meson propagating in the presence of QCD matter (14), and the cross-section for the diffractive production of vector mesons in deep inelastic scattering off nuclei (16). In the hot nuclear matter case, only the large N_c results were explicitly derived, with a diagrammatic approach which gave a more physical picture of what are the processes giving the main contribution to the dissociation of bound states. It also allowed a clear distinction between elastic and inelastic processes with respect to the target.

The two results for cold and hot matter are given by the same expression when written in terms of the saturation momentum of either the nucleus or the plasma (it is more common in this case to write $Q_s^2 = \hat{q}L$). The medium dependence enters only through this parameter. While this allowed us to make general statements, the interplay between the meson wave functions and the dipole-dipole correlator should be analyzed numerically. Even though experimentally it is not easy to appreciate the difference between elastic and inelastic processes in heavy ion collisions, we consider our result to be interesting from the theoretical point of view since we address a realistic situation where the medium can be excited by the interaction with the meson.

We obtained that the survival probability of quarkonia traversing a hot QCD medium exhibits the super-penetration feature: it decreases as $1/L$ for large medium length L . We also expect our result to be relevant when considering the production of high- p_T D and B mesons in nucleus-nucleus collisions, as these can be produced within the medium and their in-medium dissociation will contribute to the strong suppression observed at RHIC. This will be better investigated at the LHC where it should be possible to distinguish signals from charm and bottom quarks making it possible to differentiate between the two cases in a regime where we can safely rely on the eikonal approximation. Finally, an actual comparison of our results for elastic and inelastic processes is more accessible with the diffractive production of vector mesons in deep inelastic scattering off nuclei; they correspond to coherent and incoherent diffraction respectively which can be derived from our formulae.

Acknowledgments

We would like to thank Prof. A.H. Mueller for numerous discussions and helpful comments. BW is also grateful to Prof. B.-Q. Ma for useful suggestions. CM is supported by the European Commission under the FP6 program, contract No. MOIF-CT-2006-039860. BW is supported by China Scholarship Council.

-
- [1] I. Arsene *et al.* [BRAHMS Collaboration], Nucl. Phys. A **757**, 1 (2005);
 B. B. Back *et al.* [PHOBOS Collaboration], Nucl. Phys. A **757**, 28 (2005);
 J. Adams *et al.* [STAR Collaboration], Nucl. Phys. A **757**, 102 (2005);
 K. Adcox *et al.* [PHENIX Collaboration], Nucl. Phys. A **757**, 184 (2005).
 - [2] P. Jacobs and X. N. Wang, Prog. Part. Nucl. Phys. **54**, 443 (2005);
 R. Baier, D. Schiff and B. G. Zakharov, Ann. Rev. Nucl. Part. Sci. **50**, 37 (2000);
 A. Kovner and U. A. Wiedemann, arXiv:hep-ph/0304151;
 M. Gyulassy, I. Vitev, X. N. Wang and B. W. Zhang, arXiv:nucl-th/0302077.
 - [3] A. Adil and I. Vitev, Phys. Lett. B **649**, 139 (2007).
 - [4] A. Adare *et al.* [PHENIX Collaboration], Phys. Rev. Lett. **98**, 172301 (2007);
 B. I. Abelev *et al.* [STAR Collaboration], Phys. Rev. Lett. **98**, 192301 (2007).
 - [5] S. Wicks, W. Horowitz, M. Djordjevic and M. Gyulassy, Nucl. Phys. A **784**, 426 (2007).
 - [6] A. Adare *et al.* [PHENIX Collaboration], Phys. Rev. Lett. **101**, 122301 (2008).
 - [7] T. Matsui and H. Satz, Phys. Lett. B **178**, 416 (1986).
 - [8] D. Kharzeev, C. Lourenco, M. Nardi and H. Satz, Z. Phys. C **74**, 307 (1997).
 - [9] J. P. Lansberg, arXiv:0811.4005 [hep-ph].
 - [10] C. J. Benesh, J. w. Qiu and J. P. Vary, Phys. Rev. C **50**, 1015 (1994);
 J. w. Qiu, J. P. Vary and X. f. Zhang, Phys. Rev. Lett. **88**, 232301 (2002).
 - [11] H. Fujii, Phys. Rev. C **67**, 031901 (2003);
 A. M. Glenn, D. Molnar and J. L. Nagle, Phys. Lett. B **644**, 119 (2007).
 - [12] R. L. Thews, M. Schroedter and J. Rafelski, Phys. Rev. C **63**, 054905 (2001).
 - [13] F. Dominguez and B. Wu, Nucl. Phys. A **818**, 246 (2009).
 - [14] H. Kowalski, L. Motyka and G. Watt, Phys. Rev. D **74**, 074016 (2006);

- C. Marquet, R. Peschanski and G. Soyez, *Phys. Rev. D* **76**, 034011 (2007).
- [15] A. Deshpande, R. Milner, R. Venugopalan and W. Vogelsang, *Ann. Rev. Nucl. Part. Sci.* **55**, 165 (2005).
- [16] L. D. McLerran and R. Venugopalan, *Phys. Rev. D* **49**, 2233 (1994);
L. D. McLerran and R. Venugopalan, *Phys. Rev. D* **49**, 3352 (1994);
L. D. McLerran and R. Venugopalan, *Phys. Rev. D* **50**, 2225 (1994).
- [17] M. Gyulassy and X. N. Wang, *Nucl. Phys. B* **420**, 583 (1994);
M. Gyulassy, P. Levai and I. Vitev, *Phys. Rev. D* **66**, 014005 (2002).
- [18] J. P. Blaizot, F. Gelis and R. Venugopalan, *Nucl. Phys. A* **743**, 57 (2004).
- [19] J. Jalilian-Marian and Y. V. Kovchegov, *Phys. Rev. D* **70**, 114017 (2004) [Erratum-ibid. *D* **71**, 079901 (2005)].
- [20] C. Marquet, *Nucl. Phys. A* **796**, 41 (2007).
- [21] S. J. Brodsky and G. P. Lepage, *Adv. Ser. Direct. High Energy Phys.* **5**, 93 (1989).
- [22] A. Kovner and U. A. Wiedemann, *Phys. Rev. D* **64**, 114002 (2001).
- [23] H. Fujii, *Nucl. Phys. A* **709**, 236 (2002).
- [24] E. Witten, *Nucl. Phys. B* **160**, 57 (1979).
- [25] R. Baier, Y. L. Dokshitzer, A. H. Mueller, S. Peigne and D. Schiff, *Nucl. Phys. B* **484**, 265 (1997).
- [26] H. G. Dosch, T. Gousset, G. Kulzinger and H. J. Pirner, *Phys. Rev. D* **55**, 2602 (1997);
G. Kulzinger, H. G. Dosch and H. J. Pirner, *Eur. Phys. J. C* **7**, 73 (1999).
- [27] J. Hufner, C. H. Lewenkopf and M. C. Nemes, *Nucl. Phys. A* **518**, 297 (1990).
- [28] H. Fujii and T. Matsui, *Phys. Lett. B* **545**, 82 (2002).
- [29] V. L. Lyuboshitz and M. I. Podgoretsky, *JETP* **54**, 827 (1981);
L. L. Nemenov, *Sov. J. Nucl. Phys.* **34**, 726 (1981).
- [30] H. Fujii, F. Gelis and R. Venugopalan, *Nucl. Phys. A* **780**, 146 (2006).
- [31] H. Kowalski, T. Lappi and R. Venugopalan, *Phys. Rev. Lett.* **100**, 022303 (2008);
H. Kowalski, T. Lappi, C. Marquet and R. Venugopalan, *Phys. Rev. C* **78**, 045201 (2008).